JOURNAL OF GUIDANCE, CONTROL, AND DYNAMICS
Vol. 31, No. 1, January–February 2008

Development of an Active Fault-Tolerant Flight Control Strategy

Jérôme Cieslak,* David Henry,† and Ali Zolghadri‡
University of Bordeaux I, 33405 Talence, France
and
Philippe Goupil§
Airbus France, 31060 Toulouse Cedex 09, France

DOI: 10.2514/1.30551

This paper discusses the design of an active fault-tolerant flight control strategy for improvement of the operational control capability of the aircraft system. The research work draws expertise from actions undertaken within the European Flight Mechanics Action Group [FM-AG(16)] on fault-tolerant control, which develops a collaborative effort in Europe to create new fault-tolerant control technologies that significantly advance the goals of the aviation safety. The methodology is applied to a trimmable horizontal stabilizer runaway fault occurring in a large transport aircraft. The goal is to provide a self-repairing capability to enable the pilot to land the aircraft safely. The fault-tolerant control strategy works in such a way that once the fault is detected by the fault detection and isolation unit, a compensation loop is activated for safe recovery. A key feature of the proposed strategy is that the design of the fault-tolerant control loop is done independently of the nominal autopilot and the nominal flight control system in place. Nonlinear simulation results demonstrate the effectiveness of the proposed fault-tolerant control scheme.

Nomenclature

EPR•	=	thrust engine position
h	=	altitude
i_h	=	stabilizer deflection
p	=	body roll rate
q	=	body pitch rate
r	=	body yaw rate
V_{TAS}	=	true air speed
x_e	=	distance in the X_e direction
y_e	=	distance in the Y_e direction
α	=	angle of attack
β	=	angle of sideslip
$\delta_{a\bullet\bullet}$	=	aileron deflections
$\delta_{e\bullet\bullet}$	=	elevator deflections
$\delta_{f\bullet}$	=	flap deflections
$\delta_{r\bullet}$	=	rudder deflections
$\delta_{\text{sp}\bullet}$	=	spoilers
θ	=	angle of pitch
φ	=	angle of roll
ψ	=	angle of yaw

I. Introduction

THE need for increased flight safety and aircraft reliability leads to the design of reconfigurable fault-tolerant control systems. Such systems could manage adequately faulty situations and are supposed to help the crew to recover control capabilities quickly. Fault-tolerant control (FTC) strategy is one solution to tackle this problem and has received considerable attention from the control research community and aeronautical engineering in the past couple of decades (for a survey, see, for instance, [1–3]). The main objective of fault-tolerant control is to maintain the specified performance of a system in the presence of faults. Two approaches can be distinguished in this area: the passive and the active approaches. In the passive approach, the control algorithm is designed so that the system is able to achieve its given objectives, in healthy as well as in faulty situations. Unfortunately, achieving robustness to certain faults is only possible at the expense of decreased nominal performance. The active approaches react actively to fault events by using a reconfiguration mechanism. Consequently, this ensures nominal performances in fault-free situations. This is a great benefit of active FTC approaches.

An active FTC is characterized by an online and real-time fault detection and isolation (FDI) and a reconfiguration mechanism. This scheme requires its control law to react to faults through reconfiguration and FDI modules [4]. Many studies based on a possible known-fault scenario have contributed to the development of active FTC strategy for aeronautical systems (see, for instance, [3,5–7]). The goal is to maintain overall system stability and acceptable performance in spite of the occurrence of faults by reconfiguring the nominal control law when a fault is detected by the FDI unit. The FDI mechanism is supposed to detect and diagnose any relevant failure that could lead to flight performance degradation. This shall be done sufficiently early and in compliance with the stringent operational and flight dynamics constraints, to set up timely safe recovery actions and to improve the situation awareness of the crew.

The main difficulty that appears when integrating the different units to build a reliable active FTC law is that each individual subsystem is assumed to operate correctly: its output is instantaneously available to provide decisions/actions to other subsystems. This implies some interactions between the reconfigurable controller and the FDI unit (as mentioned, for instance, in [2,8,9]). To take into account this interaction, one solution could be the progressive accommodation scheme proposed in [10]. The goal is to minimize the effects of control inappropriateness during time-delay reconfiguration. However, in this case, computational burden could be a critical factor, and stability management remains a major issue.

Received 19 February 2007; revision received 18 June 2007; accepted for publication 25 July 2007.

*Ph.D. Student, Automatic Control Group, Intégration du Matériau au Système (IMS) Laboratory, 351 Cours de la Liberation; jerome.cieslak@laps.ims-bordeaux.fr (Corresponding Author).

†Associate Professor, Automatic Control Group, Intégration du Matériau au Système (IMS) Laboratory, 351 Cours de la Liberation; david.henry@laps.ims-bordeaux.fr.

‡Professor, Automatic Control Group, Intégration du Matériau au Système (IMS) Laboratory, 351 Cours de la Liberation; ali.zolghadri@laps.ims-bordeaux.fr.

§Aeronautic Engineer, Flight Control System, 316 Route de Bayonne; philippe.goupil@airbus.com.

Some works combine a fault-tolerant controller with a diagnostic filter. In [11], the authors use the standard H_∞ setting to design a nominal controller and a robust detection filter. In this configuration, the primal Youla parameterization of all stabilizing controllers is selected to ensure the fault compensation, with the assurance that closed-loop stability is maintained in the presence of fault. In [12], the dual Youla parameterization is used for determining the set of all faulty processes that can be stabilized by the (nominal) control law. It is shown that both fault diagnosis and fault-tolerant control can be combined in the same architecture, and this is an interesting framework for analyzing the relationship between FDI and FTC. However, to cope with performance degradation when faults are not detected by the FDI, the authors proposed to activate the fault-tolerant controller all the time. As a consequence, their approach is equivalent to a passive FTC scheme. Other works are based on linear parameter-varying (LPV) techniques [13,14]. The idea is to use the residual output of the FDI scheme jointly with some subspace of the system states as scheduling parameters of the LPV fault-tolerant controller.

In this paper, an attempt is made to provide an active FTC strategy that addresses the aforementioned issues. The application is related to ongoing research is undertaken within a Group for Aeronautical Research and Technology in Europe (GARTEUR) program to assess the capability of active FTC schemes on a realistic design problem.

The proposed active FTC strategy is based on H_∞ control theory and it is applied to an aircraft suffering from degraded stabilizer control effectiveness. A key feature of the proposed strategy is that the design of the FTC loop is done independently of the nominal autopilot and the nominal flight control system (FCS) already in place. The paper is organized as follows. Section II introduces FTC concepts. Section III is devoted to the analysis of the proposed FTC architecture, and Sec. IV presents the application and simulation results.

II. Problem Statement

Motivated by several aircraft accidents at the end of the 1970s, in particular, the crash of an American Airlines DC-10 in Chicago in 1979, research on self-repairing or reconfigurable fault-tolerant flight control has become a very active research topic in the last decades. In this context, the European Flight Mechanics Action Group 16 [FM-AG(16)] on fault-tolerant control GARTEUR program was established to demonstrate the capability and viability of reconfiguration schemes on a realistic nonlinear design problem. As part of this research, a simulation benchmark based on the Boeing 747-100/200 large transport aircraft was developed for the integrated assessment of FTC methods [15–17]. This aircraft was chosen because its wide array of characteristics (26 control surfaces and 4 jet engines) makes it representative of most of the commercial airplanes flying today. The test scenarios that are an integral part of the benchmark were selected to provide challenging assessment criteria to evaluate the potential of the FTC methods investigated. The benchmark test maneuvers correspond to the landing approach. A schematic overview of these maneuvers is given in Fig. 1.

In the benchmark, the pilot commands are replaced by signals generated by the benchmark scenario generator. The aircraft is a B747 fitted with its standard autoflight system, as shown in Fig. 2. The autoflight system integrates a longitudinal and a lateral controller. Each controller contains inner and outer loops. Referring to Fig. 2, the autoflight system consists of the FCS that forms the inner control loop and an outer loop represented by the autopilot system (autothrottle is not implemented yet). In addition, an onboard FDI unit was placed within the simulator. Five faulty scenarios (essentially actuator faults) and the El Al Flight 1862 in Bijlmermeer in 1992 [18] catastrophic accident are considered in the benchmark.

The faulty situation investigated in this paper consists of the motion of the extreme positions of the trimmable horizontal stabilizer (THS) surface at the maximum rate limit (i.e., $+0.5\,\mathrm{deg/s}$), occurring when the airplane is in normal flight (i.e., first part of the maneuver, see Fig. 1). More precisely, the THS fault corresponds to a hardware malfunction. Hence, we assume that it is not possible to act on the faulty THS surface to accommodate it or put it into its neutral position. For the studied flight trajectory, the aircraft is in the so-called altitude select pitch mode. Consequently, the dynamic behavior of the transport aircraft is given by the longitudinal motion.

The goal we pursue is to develop a FTC scheme to accommodate stabilizer failure using the remaining control surfaces (the elevator surfaces). It should be pointed out that the maximum deflection in the positive direction of the THS surface (i.e., $+3$ deg) and to a negative position (up to -5 deg) can be fully compensated using this strategy. However, the movement to its extreme negative position (i.e., -12 deg) cannot be compensated, due to the physical limitations of the elevator deflections.

Following the basic ideas presented in [19], we propose to tackle the design of the FTC loop according to the block diagram of Fig. 3. The proposed reconfigurable flight control and safety recovery scheme is made of three parts: an FDI part represented by $H_y(s)$, $H_u(s)$, and decision-making rules, which continuously generates a fault-indicating signal r; an FTC part represented by $\tilde{K}(s)$ which generates an additional control signal $\tilde{u}$ to be added to the nominal control signal u_o in a faulty situation; and a FTC activation mechanism to activate the FTC strategy. Once again, the overall FTC strategy works in such a way that in a fault-free situation, the FTC

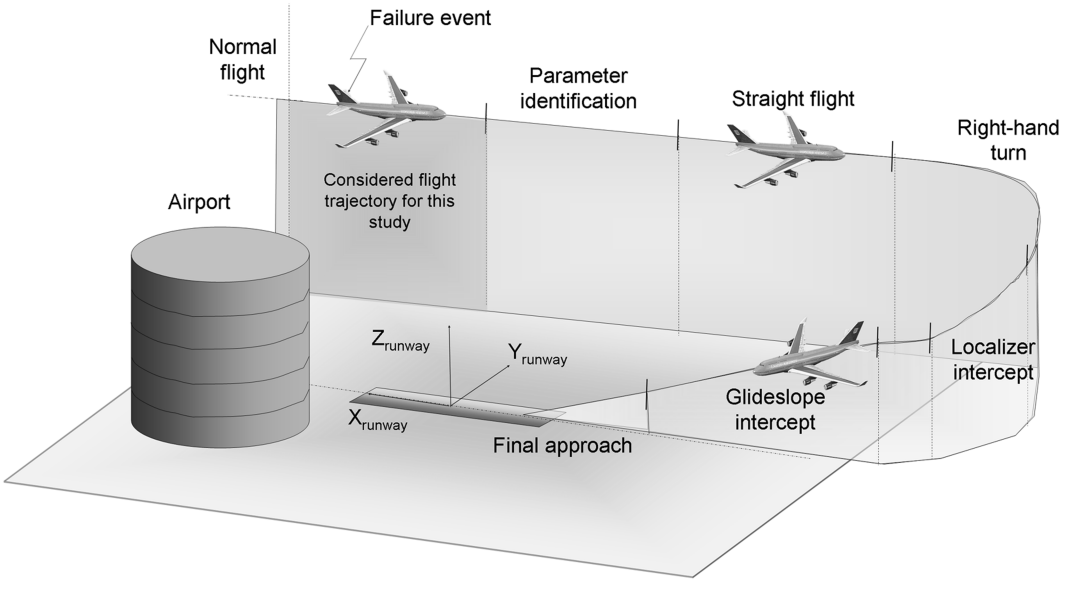

Fig. 1 Test maneuvers studied in the benchmark.

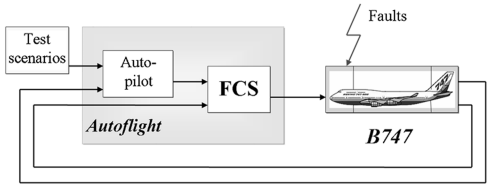

Fig. 2 Benchmark setup.

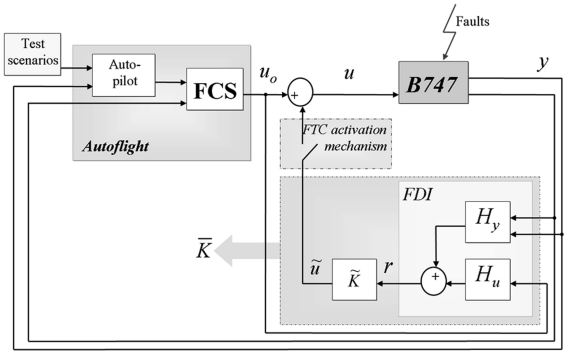

Fig. 3 Benchmark setup associated with the proposed AFTC strategy.

loop is not activated, leaving the aircraft controlled only by the autoflight control system. When the FTC strategy is activated, the control law is reconfigured by adding the signal $\tilde{u}$ to the nominal control signal u_o. The activation of this loop is done by using a switching logic; that is, the autoflight control system is not removed when no fault is present and, consequently, the overall scheme ensures nominal flight performance in fault-free situations. This is one major advantage of the proposed method.

This proposed active FTC architecture implies some important issues. The first question concerns the activation delay of the strategy FTC. During this time interval, the faulty system is controlled by the nominal control law that has not been designed for faulty situations. This problem is also highly related to the time-delay detection of the FDI part. In this paper, we will present a method that addresses this problem efficiently. Next, as can be seen in Fig. 3, in fault-free situation, the FTC scheme is in open loop. Then an important requirement for FTC scheme is that the interconnection of $H_y(s)$, $H_u(s)$, and $\tilde{K}(s)$, depicted in Fig. 3, must be stable. Because $H_y(s)$ and $H_u(s)$ are stable detection filters, this problem is equivalent to the stability requirement of $\tilde{K}(s)$. This will be discussed in Sec. IV. Another important aspect is the availability of the FDI mechanism. In the case of analytical redundancy, the representations of the filters $H_y(s)$ and $H_u(s)$ are also available. The decision-making rules that activate the FTC strategy are then monitored by the residual signal r. The diagram in Fig. 3 can then be represented by the diagram of Fig. 4, in which $K_n(s)$ is the autoflight control system and $G(s)$ is the model of aircraft dynamics. The FTC design problem is now equivalent to the design of a dynamic fault-tolerant controller $\tilde{K}(s)$ that ensures input/output insensitivity in some sense, despite the presence of the fault.

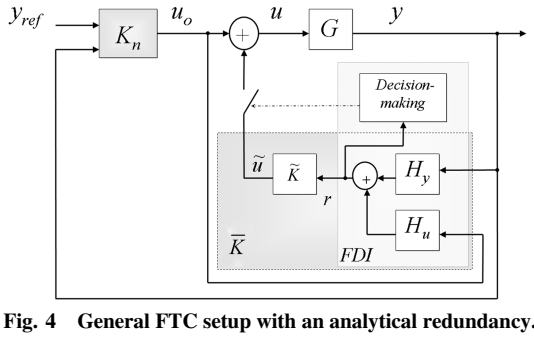

Fig. 4 General FTC setup with an analytical redundancy.

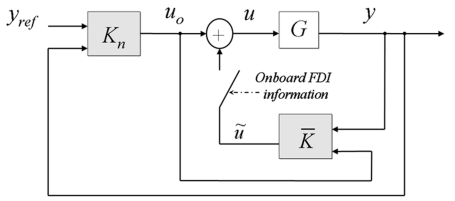

Fig. 5 General FTC setup with an onboard FDI scheme.

Problem 1: Suppose that the faulty system is stabilizable. The goal is to design a stable controller $\tilde{K}(s)$ to produce the new control signal:

$$u(t) = u_o(t) + \tilde{K}(s)r(t) \tag{1}$$

such that the stability of the feedback system and the required control objectives are guaranteed for the considered THS fault. Using an H_∞ formulation, this means that $\tilde{K}(s)$ should satisfy the following constraint:

$$\|F_l[P_1(\mathrm{s}), \tilde{K}(\mathrm{s})]\|_\infty < \gamma_1 \tag{2}$$

where $P_1(s)$ is deduced from $K_n(s)$, $G(s)$, $H_y(s)$, and $H_u(s)$ using some linear-fractional manipulations, and γ_1 denotes some FTC performance level to achieve. Here, $F_l[P_1(\mathrm{s}), \tilde{K}(\mathrm{s})]$ corresponds to the lower linear-fractional transformation of $P_1(s)$ by $\tilde{K}(s)$.

When the FDI mechanism is available onboard, the FTC problem can be seen as the design of a filter $\bar{K}(s)$ (Fig. 5). The onboard FDI unit is also used to manage the activation switch. In this case, the synthesis problem can be formulated as follows:

Problem 2: Suppose that the faulty system is stabilizable. The goal is to design a stable controller $\bar{K}(s)$ to produce the new control signal:

$$\tilde{u}(t) = \bar{K}(s)\begin{pmatrix} y(t) \\ u_o(t) \end{pmatrix} \tag{3}$$

such that the stability of the feedback system and the required control objectives are guaranteed for the considered THS fault. Using an H_∞ formulation, this means that $\bar{K}(s)$ should verify

$$\|F_l[P_2(\mathrm{s}), \bar{K}(\mathrm{s})]\|_\infty < \gamma_2 \tag{4}$$

where $P_2(s)$ is deduced from $K_n(s)$ and $G(s)$ after some linear-fractional algebra manipulations, and γ_2 represents some performance level to achieve.

Remark 1: Referring to the setup diagrams in Fig. 4 and 5, it is natural to ask about the stability of the FTC loop due to the presence of the switch. Here, we assume that once a fault is detected, the switch is definitively activated and the compensation signal $\tilde{u}$ remains active all the time. The remaining problem then concerns the transient behavior of $\tilde{u}$. To avoid bumps, a solution to manage this problem is given in Appendix B.

III. Analysis of the FTC System

Before proceeding to the design of the FTC loop for the FM-AG (16) benchmark, the structure of the FTC system presented in Fig. 4 is analyzed to highlight some interesting features with respect to the interaction between the FDI and FTC units.

A. Analysis of the FTC Loop

Consider the general setup shown in Fig. 5. Let (A, B, C, D), $(\tilde{A}, \tilde{B}, \tilde{C}, \tilde{D})$, (A_u, B_u, C_u, D_u), and (A_y, B_y, C_y, D_y) be the state-space representations of $G(s)$, $\tilde{K}(s)$, $H_u(s)$, and $H_y(s)$, respectively.

The FTC loop state-space model $\bar{P}(s)$, which includes $G(s)$, $\tilde{K}(s)$, $H_u(s)$, and $H_y(s)$, is given by

$$\bar{P}: \begin{cases} \begin{pmatrix} \dot{x}_c \\ \dot{x}_u \end{pmatrix} = \begin{pmatrix} A_{11} & A_{12} \\ 0 & A_u \end{pmatrix}\begin{pmatrix} x_c \\ x_u \end{pmatrix} + \begin{pmatrix} B_1 \\ B_u \end{pmatrix} u_o \\ y = \begin{pmatrix} C_1 & C_2 \end{pmatrix}\begin{pmatrix} x_c \\ x_u \end{pmatrix} + (D_{\bar{p}})u_o \end{cases} \tag{5}$$

where the matrices $A_{11}, A_{12}, B_1, C_1, C_2$, and $D_{\bar{P}}$ are deduced from the preceding state-space representations as follows:

$$A_{11} = \begin{pmatrix} A + BM\tilde{D}D_yC & BM\tilde{C} & BM\tilde{D}C_y \\ \tilde{B}D_y(C + DM\tilde{D}D_yC) & \tilde{A} + \tilde{B}D_yDM\tilde{C} & \tilde{B}(I + D_yDM\tilde{D})C_y \\ B_y(I + DM\tilde{D}D_y)C & B_yDM\tilde{C} & A_y + B_yDM\tilde{D}C_y \end{pmatrix} \tag{6}$$

$$A_{12} = \begin{pmatrix} BM\tilde{D}C_u \\ \tilde{B}(I + D_yDM\tilde{D})C_u \\ B_yDM\tilde{D}C_u \end{pmatrix} \tag{7}$$

$$B_1 = \begin{pmatrix} BM(I + \tilde{D}D_u) \\ \tilde{B}[D_u + D_yDM(I + \tilde{D}D_u)] \\ B_yDM(I + \tilde{D}D_u) \end{pmatrix} \tag{8}$$

$$C_1 = \begin{pmatrix} C + DM\tilde{D}D_yC & DM\tilde{C} & DM\tilde{D}C_y \end{pmatrix} \tag{9}$$

$$C_2 = (DM\tilde{D}C_u) \tag{10}$$

$$D_{\bar{P}} = DM(I + \tilde{D}D_u) \tag{11}$$

$$M = (I - \tilde{D}D_yD)^{-1} \tag{12}$$

and $x_c = \begin{pmatrix} x^T & \tilde{x}^T & x_y^T \end{pmatrix}^T$; $x, \tilde{x}, x_y$, and x_u are, respectively, the state of $G(s)$, $\tilde{K}(s)$, $H_y(s)$, and $H_u(s)$.

From Eq. (5), it can be seen that the poles of $\bar{P}(s)$ are given by the eigenvalues of A_{11} and A_u. Note that the expression of A_{11} does not contain A_u, B_u, C_u, or D_u matrices; it follows that $H_u(s)$ (stable filter) has no effect on the stability of $\bar{P}(s)$. This analysis justifies the choice to take the signal u_o for the FDI instead of u. In the latter case, an internal loop appears, vanishing the property observed here.

B. Analysis of the Overall Loop

Now we consider the diagram of Fig. 5, in which the state-space representations of $K_n(s)$ and $\bar{P}(s)$ are given by (A_n, B_n, C_n, D_n) and $(A_{\bar{P}}, B_{\bar{P}}, C_{\bar{P}}, D_{\bar{P}})$, respectively. Let x_n be the state vector of $K_n(s)$. Direct calculations lead to the following closed-loop state-space model:

$$\begin{cases} \begin{pmatrix} \dot{x}_{\bar{P}} \\ \dot{x}_n \end{pmatrix} = A_T \begin{pmatrix} x_{\bar{P}} \\ x_n \end{pmatrix} + B_T y_{\text{ref}} \\ y = C_T \begin{pmatrix} x_{\bar{P}} \\ x_n \end{pmatrix} + D_T y_{\text{ref}} \end{cases} \tag{13}$$

where A_T, B_T, C_T, and D_T are given by

$$A_T = \begin{pmatrix} A_{\bar{P}} + B_{\bar{P}}D_{n_y}NC_{\bar{P}} & B_{\bar{P}}C_n + B_{\bar{P}}D_{n_y}ND_{\bar{P}}C_n \\ B_{n_y}NC_{\bar{P}} & A_n + B_{n_y}ND_{\bar{P}}C_n \end{pmatrix} \tag{14}$$

$$B_T = \begin{pmatrix} B_{\bar{P}}(I + D_{n_y}ND_{\bar{P}}D_n)D_{n_{\text{ref}}} \\ B_{n_{\text{ref}}} + B_{n_y}ND_{\bar{P}}D_{n_{\text{ref}}} \end{pmatrix} \tag{15}$$

$$C_T = \begin{pmatrix} NC_{\bar{P}} & ND_{\bar{P}}C_n \end{pmatrix} \tag{16}$$

$$D_T = (ND_{\bar{P}}D_{n_{\text{ref}}}) \tag{17}$$

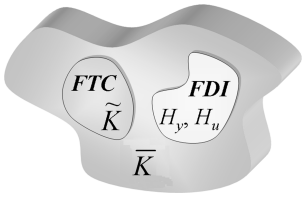

Fig. 6 Set of all admissible FDI/FTC units.

$$N = (I - D_{\bar{P}}D_{n_y})^{-1} \tag{18}$$

$$B_n = \begin{pmatrix} B_{n_{\text{ref}}} & B_{n_y} \end{pmatrix} \tag{19}$$

$$D_n = \begin{pmatrix} D_{n_{\text{ref}}} & D_{n_y} \end{pmatrix} \tag{20}$$

and $x_{\bar{P}} = \begin{pmatrix} x^T & \tilde{x}^T & x_y^T & x_u^T \end{pmatrix}^T$.

Equation (13) shows that the stability of the overall loop depends on the stability of the FDI filter. This is an expected and rather evident result. Then Eq. (13) reveals that FDI and FTC dynamics are highly coupled.

C. Some Outlines for the Design

The preceding analysis allows an outline for the design of an integrated FTC/FDI unit. A nice feature of the proposed FTC architecture presented in Fig. 3 is that $\bar{K}(s)$ filter can be seen as the set of all admissible FDI/FTC units that achieves some level of performance γ_2. This suggests the following design procedure. First, design $\bar{K}(s)$ according to some FTC objectives (see Problem 2). Once $\bar{K}(s)$ is designed, the challenge is to deduce from $\bar{K}(s)$ the FDI parts $H_y(s)$ and $H_u(s)$ and the FTC part $\tilde{K}(s)$. The suggested procedure will consist of designing $H_y(s)$ and $H_u(s)$ and then to integrate the FDI performance specifications into the FTC design procedure. Thus, the obtained FDI/FTC couple is the solution of the problem of integrated FTC/FDI units design, if and only if this couple belongs to the set $\bar{K}(s)$; that is, if

$$\|F_l\{P_2(s), F_l[F(s), \tilde{K}(s)]\}\|_\infty < \gamma_2 \tag{21}$$

where $F(s)$ is the diagnostic filter composed by the $H_y(s)$ and $H_u(s)$ filters. This situation can be illustrated as shown in Fig. 6.

IV. FM-AG(16) Garteur FTC Problem

We now consider the problem of designing the FTC loop to compensate THS runaway failures. We assume that an onboard-fault-diagnosis unit that detects and isolates this fault type is available. Thus, the problem becomes that of designing the filter $\bar{K}(s)$ such that Eqs. (3) and (4) are achieved.

A. Modeling the Boeing 747 Aircraft Dynamics

The Boeing 747-100/200 model includes aircraft aerodynamic model and engines. In addition, actuator and sensor characteristics are taken into account, together with models for wind, atmospheric turbulence, and faults [15,16,20]. The aerodynamic forces and moments are defined in terms of aerodynamic coefficients. These coefficients are stated in the form of lookup tables. They are functions of a wide set of parameters (pitch angle, angle of attack, true airspeed, altitude, etc.). The dimension of the aircraft output vector is 142. However, all output signals are not necessary to control the aircraft. Indeed, the FCS (inner control loop) uses only 16 measured signals and the autopilot that corresponds to the outer control loop needs 67 measured signals. The dynamic behavior of the aircraft is described by a nonlinear state representation:

$$\dot{x}_{\mathrm{NL}}(t) = f[x_{\mathrm{NL}}(t), u_{\mathrm{NL}}(t)] \tag{22}$$

$$y_{\mathrm{NL}}(t) = g[x_{\mathrm{NL}}(t), u_{\mathrm{NL}}(t)] + v(t) \tag{23}$$

where x_{NL}, u_{NL}, and y_{NL} are the state, input, and output vectors, respectively, of the full aircraft nonlinear model [the input and state components are given in Appendix A (see Tables A1 and A2)], and v are the measurement noises that are assumed to be normal Gaussian-distributed random signals. The interested reader can refer to [15] for a complete description of the aircraft output vector. In this formulation, we assume that model parameters (mass and inertia) are fixed to their nominal values.

Once a trim condition is established for the nonlinear aircraft model, a linear model is generated to capture the dynamics around the point: $h = 1000$ m; $V_{\mathrm{TAS}} = 133.8$ m/s; $m = 263,000$ kg; and $M = 0.3977$, where h, V_{TAS}, m, and M denote, respectively, the altitude, the aircraft velocity, the mass of the aircraft, and the Mach number.

Simplified models for the longitudinal and lateral modes can then be derived to obtain a better physical insight into the modes and their interactions. These models are widely used in aeronautical engineering and are not developed here. Because the aircraft stays in the pitch mode for the considered fault, only the longitudinal mode is considered. Here, the longitudinal mode is represented by the following state equations:

$$\begin{cases} \dot{x}(t) = Ax(t) + Bu(t) \\ y(t) = Cx(t) + v(t) \end{cases} \tag{24}$$

where the longitudinal state vector is defined by $x = (q, V_{\mathrm{TAS}}, \alpha, \theta, h)^T$; $u = (\delta_{e\bullet\bullet}, i_h)^T$ is the control input vector; and $y = (q, V_{\mathrm{TAS}}, \theta, h, \dot{h})^T$ is the measured output vector (see Appendix A for the definition of all variables).

Taking into account the THS runaway faults, the following linear state-space model is derived from Eq. (24):

$$\begin{cases} \dot{x}(t) = Ax(t) + B_e u(t) + B_f f_{\mathrm{THS}}(t) \\ y(t) = Cx(t) + v(t) \end{cases} \tag{25}$$

where B_e and B_f are matrices of appropriate dimensions deduced from B. The input signals $u = \delta_{e\bullet\bullet}$ correspond to the elevator defections, and $f_{\mathrm{THS}} = i_h$ denotes the THS fault [hardware malfunction (see Sec. II)]. Note that this model is clearly an approximation of the real faulty behavior of the aircraft. Figure 7 shows linear and nonlinear simulation results. It can be seen that the linearized model responses are close to the responses of the nonlinear model given in Eqs. (22) and (23).

B. Modeling the Autoflight Control System

The autoflight system integrates a longitudinal and a lateral controller [21]. For the considered flight trajectory (longitudinal motion), the implemented autoflight control system is represented in Fig. 8. It can be seen on the figure that the elevator control system is composed of two control loops. The inner and outer control loops adequately manage the elevator control surface $\delta_{e\bullet\bullet}$ to control the altitude. The THS position is controlled by thumb switches on the pilot and copilot control wheels (actions given by the test scenarios). As classically designed in the aeronautical engineering, it can be seen that the autoflight control system remains in a gain-schedule-based controller, in which the scheduling parameters are h and V_{TAS}. K_1, K_2, K_3, K_4, K_5, and K_6 are constant gains and $K_7(s)$ and $K_8(s)$ are dynamic controllers designed to keep stability and performances during a longitudinal flight.

Because it is assumed that V_{TAS} keeps (almost) constant value during the considered flight trajectory, it is obvious to obtain (from the structure illustrated in Fig. 8) a linear model $K_n(s)$ for the autoflight system. Thus, it turns out that the global model of the Boeing 747 (i.e., aircraft, actuator, sensor dynamics, and autoflight system) has the structure illustrated in Fig. 5.

C. Design of $\bar{K}(s)$

The problem is now to design a stable controller $\bar{K}(s)$ such that

$$\|F_l[P_2(\mathrm{s}), \bar{K}(\mathrm{s})]\|_\infty < \gamma_2$$

(see the discussion in Sec. II). To this end, a mixed-sensitivity H_∞ synthesis is proposed. The setup diagram used for the design problem is given on Fig. 9.

$W_{p1}(s)$ and $W_{p2}(s)$ are weighting functions used to shape the transfer functions $S_{\mathrm{FTC}}(s)$ and $R_{\mathrm{FTC}}(s)$ given by

$$S_{\mathrm{FTC}}(s) = \left[I - G_u(s)\left(K_n(s) + \bar{K}(s)\begin{bmatrix} I & \\ & K_n(s) \end{bmatrix}\right)\right]^{-1} G_f(s) \tag{26}$$

$$R_{\mathrm{FTC}}(s) = \left(K_n(s) + \bar{K}(s)\begin{bmatrix} I & \\ & K_n(s) \end{bmatrix}\right) S_{\mathrm{FTC}}(s) \tag{27}$$

where the transfer functions G_u and G_f are, respectively, given by

$$G_u(s) = C(sI - A)^{-1}B_e$$

and

$$G_f(s) = C(sI - A)^{-1}B_f$$

A, B_e, B_f, and C matrices are defined according to Eq. (25). S_{FTC} and R_{FTC} also refer, respectively, to the faulty sensitivity function and the faulty sensitivity function of the controlled input.

Using some linear-fractional algebra manipulations, the problem illustrated in Fig. 9 becomes the problem presented Fig. 10. Then $\bar{K}(s)$ can be computed by using any standard robust control design method. However, as outlined in Sec. II, $\bar{K}(s)$ operates in an open-loop manner in a fault-free situation. Therefore, $\bar{K}(s)$ must be designed to be stable. Linear matrix inequality (LMI)-based solutions exist in the literature [22,23] that address the stability of $\bar{K}(s)$. To avoid duplicating published materials, we will not present the solution. The interested reader can refer to [22,23] for necessary backgrounds.

The weighting function $W_{p1}(s)$ was chosen to impose a small damping ratio on altitude h (m) and pitch rate q (rad/s) in the faulty situation, and $W_{p2}(s)$ was fixed to take into account actuator saturation phenomena. More precisely, $W_{p2}^{-1}(s)$ is a low-pass filter used to attenuate the energy of the control signal applied to elevator surfaces such that the control-signal behavior keeps smooth (high-frequency filter action). The final choice for $W_{p1}(s)$ and $W_{p2}(s)$ are

$$\begin{aligned} W_{p1}(s) &= \left(5, 6.10^4 \frac{5s+1}{1.10^4 s+1}, 1.10^5 \frac{12,5s+1}{25.10^5 s+1}\right) \\ &= [W_{11}(s), W_{14}(s)] \end{aligned} \tag{28}$$

$$W_{p2}(s) = \mathrm{diag}\left(0,1\frac{0,2s+1}{1,4.10^{-2}s+1}, 0,1\frac{0,2s+1}{1,4.10^{-2}s+1}, 0,1\frac{0,2s+1}{1,4.10^{-2}s+1}, 0,1\frac{0,2s+1}{1,4.10^{-2}s+1}\right) \tag{29}$$

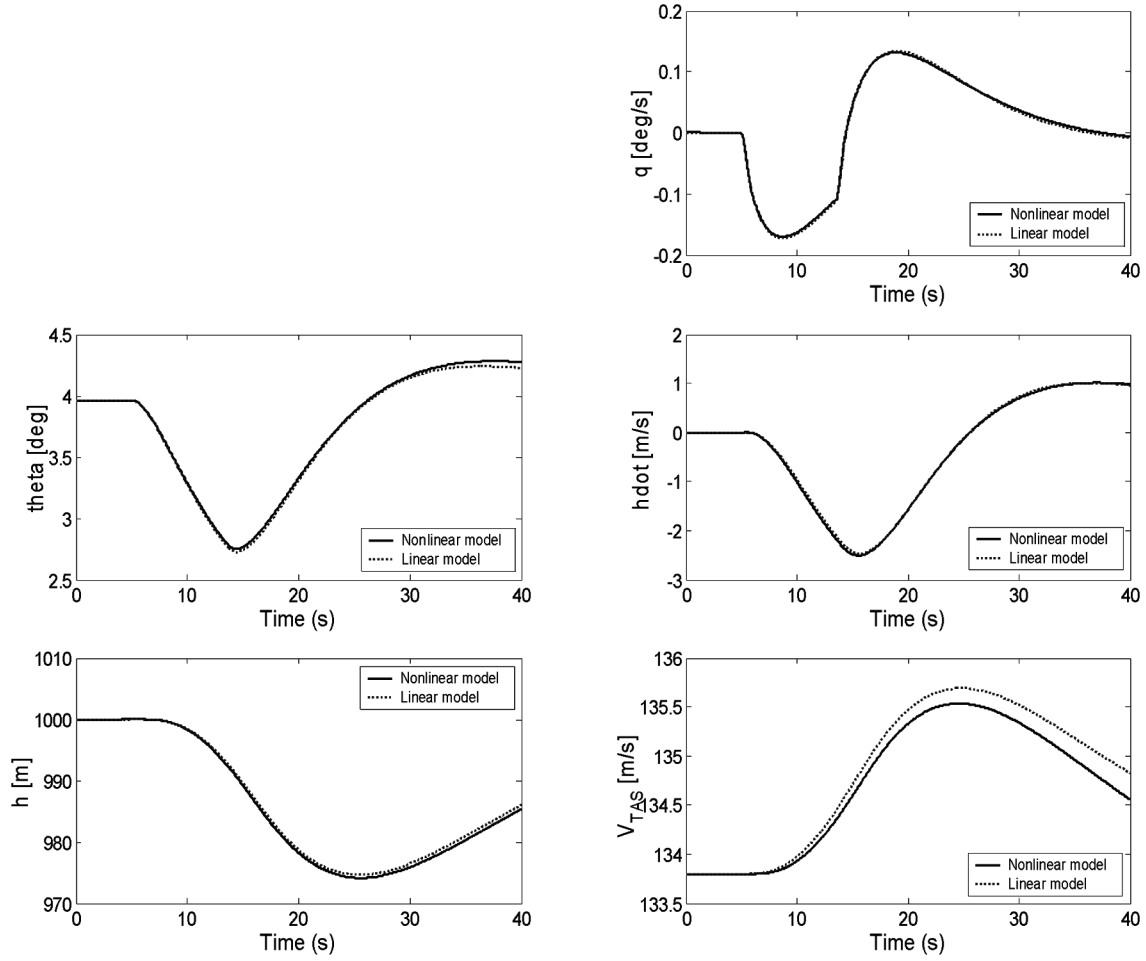

Fig. 7 Dynamic behavior of linear and nonlinear models for THS fault and without noises.

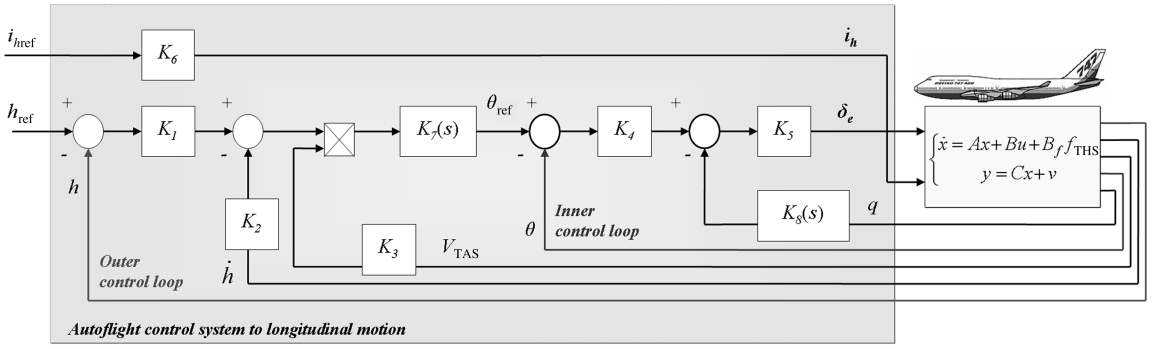

Fig. 8 Autoflight control system for the considered flight trajectory.

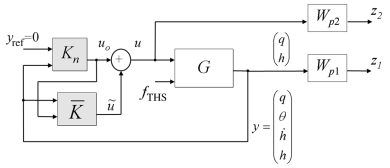

Fig. 9 FTC synthesis problem.

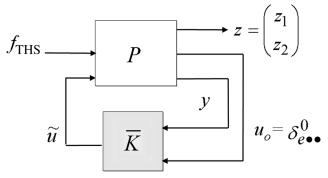

Fig. 10 Design of the fault-tolerant controller.

$\bar{K}(s)$ is then synthesized following the method described earlier. The SDPT3-3.02 solver [24] is used for numerical computations. Figure 11 shows frequency responses obtained with $\bar{K}(s)$.

As can be seen,

$$\bar{\sigma}[T_{f_{\text{THS}}\to h}(j\omega)] < \left|W_{14}^{-1}(j\omega)\right| \qquad \forall\ \omega$$

$$\bar{\sigma}[T_{f_{\text{THS}}\to q}(j\omega)] < \left|W_{11}^{-1}(j\omega)\right| \qquad \forall\ \omega$$

and

$$\bar{\sigma}[T_{f_{\text{THS}}\to \delta_e}(j\omega)] < \left|W_{p2}^{-1}(j\omega)\right| \qquad \forall\ \omega$$

indicating that the computed FTC controller $\bar{K}(s)$ achieves the desired performance level.

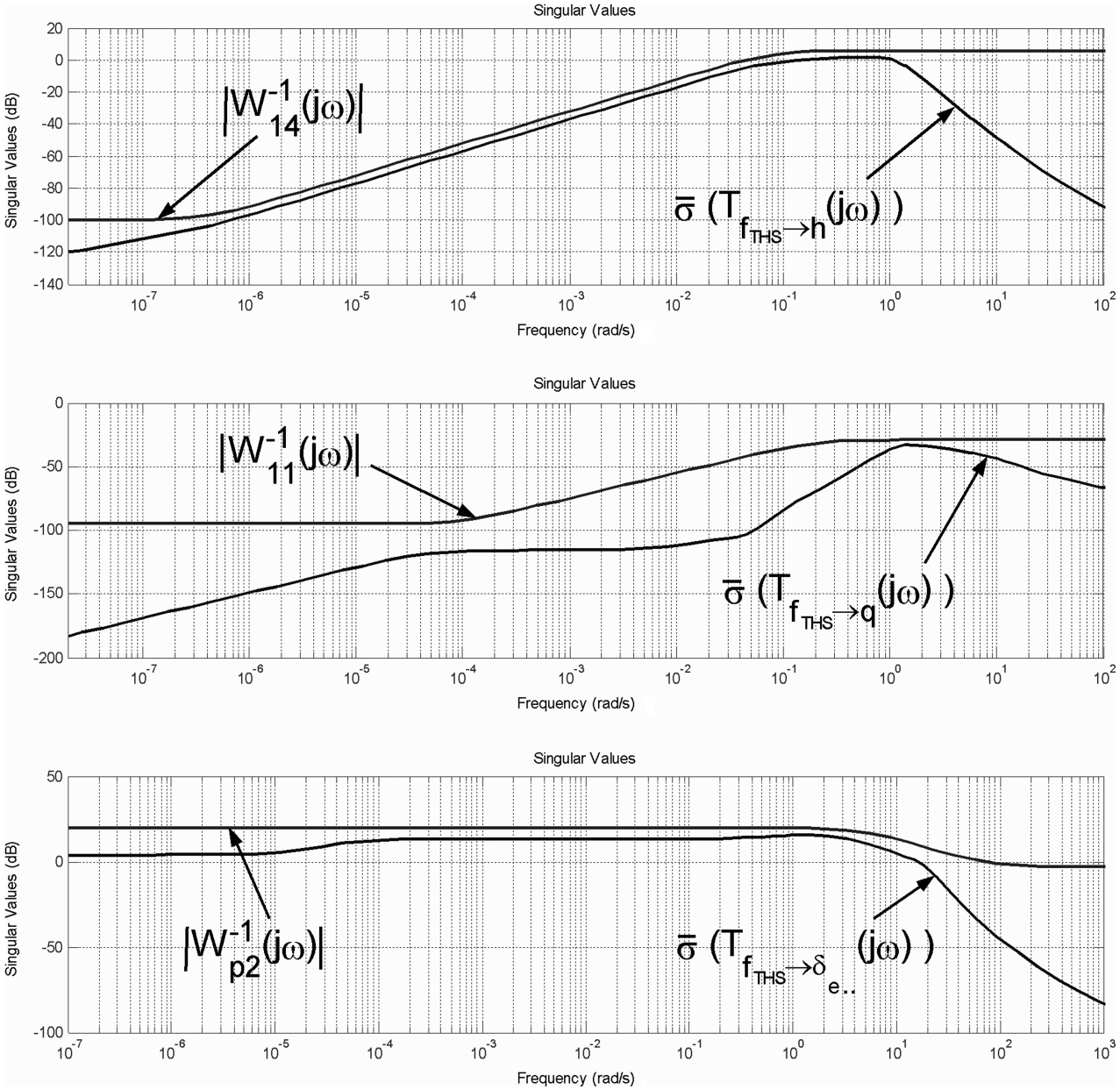

Fig. 11 Post analysis of $\bar{K}(s)$.

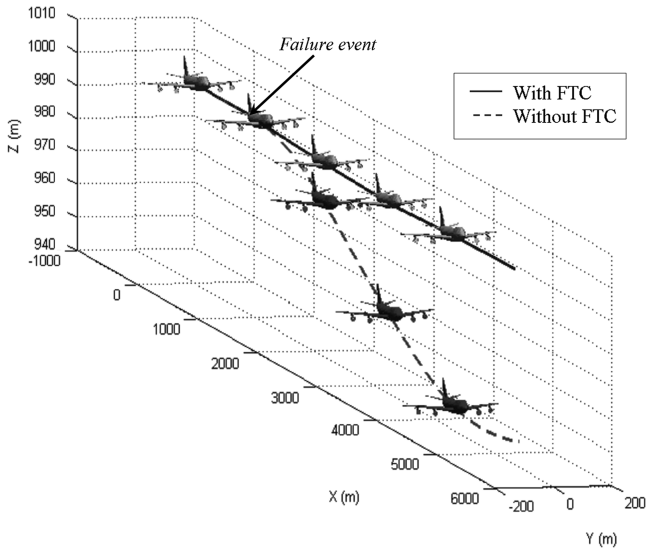

Fig. 12 Aircraft response: THS runaway fault (+3 deg).

D. Nonlinear Simulation Results

The controller $\bar{K}(s)$ is implemented within the FM-AG(16) GARTEUR nonlinear simulator of the Boeing 747 aircraft of Fig. 5.

The faulty scenario corresponds to the THS fault (the THS surface moves quickly to the extreme position of +3 deg) occurring at $t = 5$ s. To emphasize the benefit of the proposed FTC scheme, the same simulation is carried out when the system is only controlled by the standard B747 control system (no FTC). Figure 12 illustrates the behavior of the aircraft for the system controlled by the autoflight control system alone and when FTC strategy is engaged.

It can be seen that with the designed FTC scheme, the aircraft maintains normal flight trajectory (i.e., the aircraft stays at the selected altitude). However, when the aircraft is controlled by the conventional FCS, it does not stay at the desired altitude. Figure 13 more precisely illustrates the behavior of the aircraft via the altitude h, the pitch rate q, the velocity V_{TAS}, the pitch angle θ, the altitude rate $\dot{h}$, and the control signals $\delta_{e\bullet\bullet}$ for the two control schemes. As can be seen from Fig. 13, when the FTC scheme is in place, the controlled system keeps acceptable flying condition (i.e., quick compensation of the fault, with the damping ratio almost null on input/output system signals).

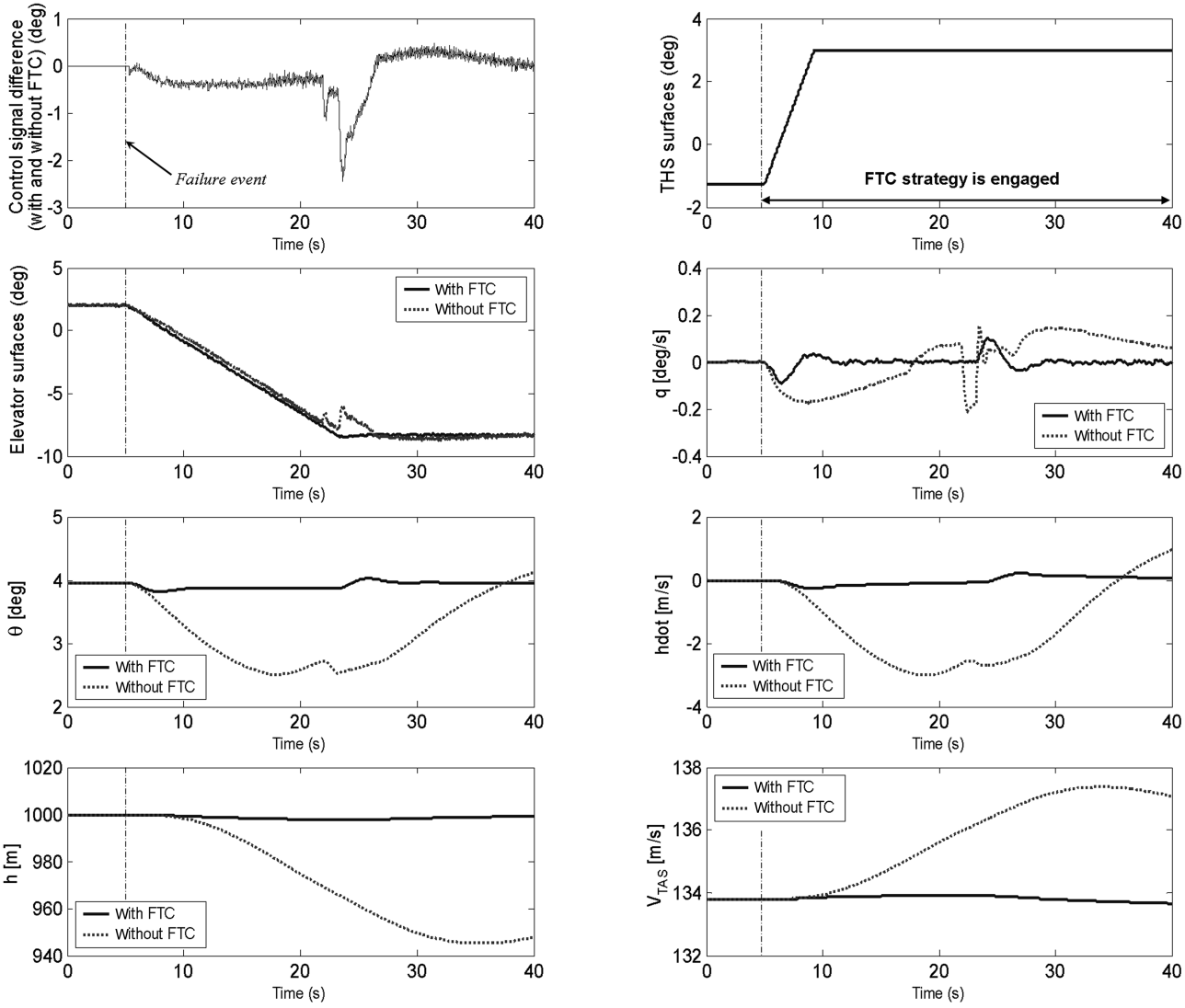

Fig. 13 Aircraft responses due to THS runaway fault (+3 deg).

Furthermore, it can be seen that, as expected, the elevator deflections do not violate the position and rate limits (the deflection and rate limits for the elevators are $[-23\,\text{deg};\ +17\,\text{deg}]$ and $\pm 37\,\text{deg}/\text{s}$, respectively).

Figure 14 illustrates the behavior of the load factor n_z. As can be seen, the magnitude of undesirable transients on n_z caused by the occurrence of fault is reduced when the FTC strategy is in place. From a practical point of view, the aircraft exhibits smaller excursions in altitude, airspeed, etc. Note that when the aircraft is only controlled by the conventional autoflight control system, undesirable transient behaviors appear between 20 and 27 s. A

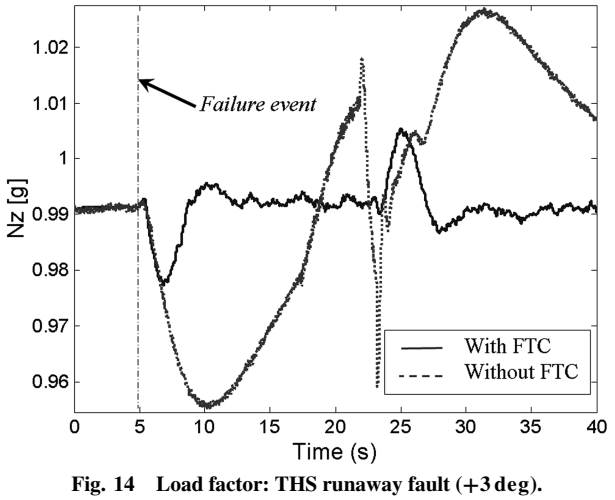

Fig. 14 Load factor: THS runaway fault (+3 deg).

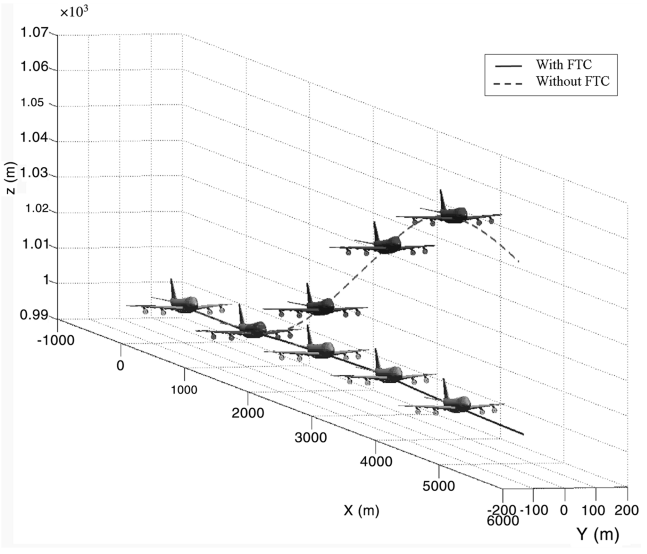

Fig. 15 Aircraft response: THS runaway fault (−5 deg).

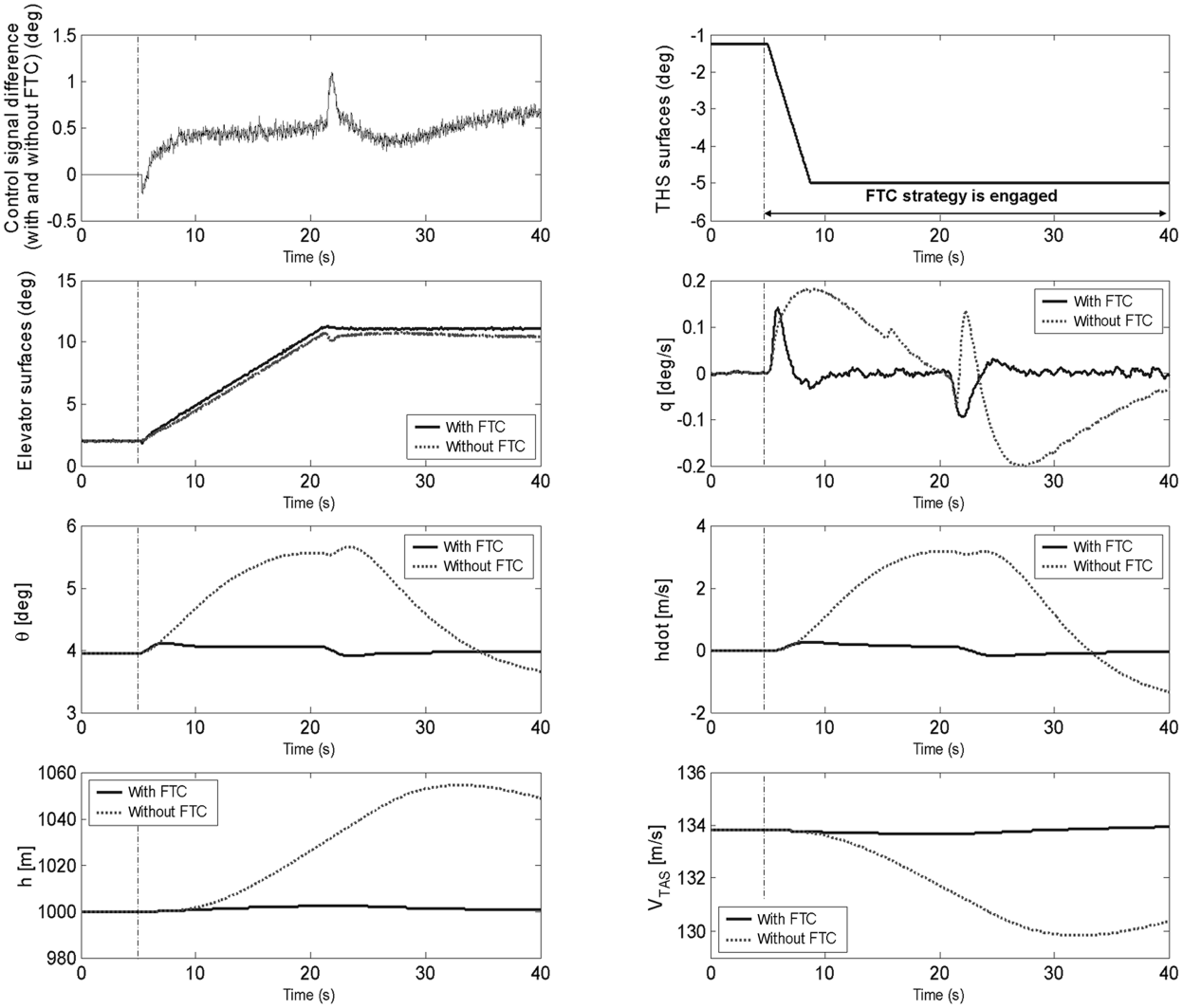

Fig. 16 Aircraft responses due to THS runaway fault (−5 deg).

deeper investigation into these situations reveals an inappropriate gain scheduling of the autoflight.

Remark 2: Following Remark 1, the activation of the switch may cause some undesirable bumps. To overcome this problem, a solution is discussed in Appendix B. Here, such a bumpless solution was revealed to be unnecessary.

Another simulation is performed when the THS goes to the negative position −5 deg at the maximum rates. Figures 15–17 illustrate the results. As can be seen, the FTC law performs as expected.

Finally, another failure mode for the THS surface is studied. The new faulty scenario corresponds to an oscillatory scenario occurring at $t = 5$ s. The time period and the amplitude of the oscillation are fixed to 34 s and 4 deg, respectively. These failure characteristics were chosen because they can degrade the aircraft handling quality.

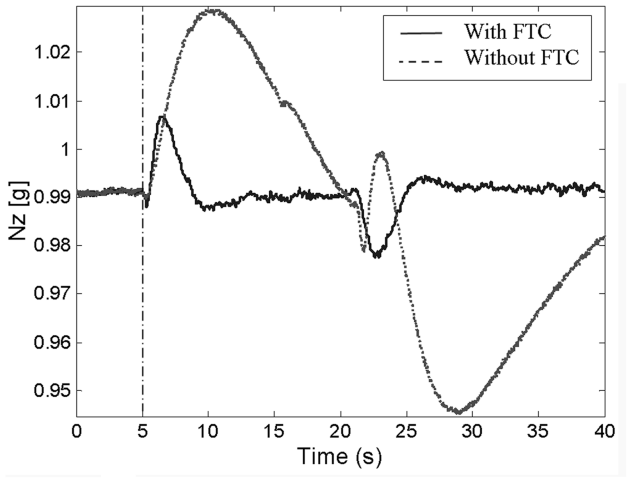

Fig. 17 Load factor: THS runaway fault (−5 deg).

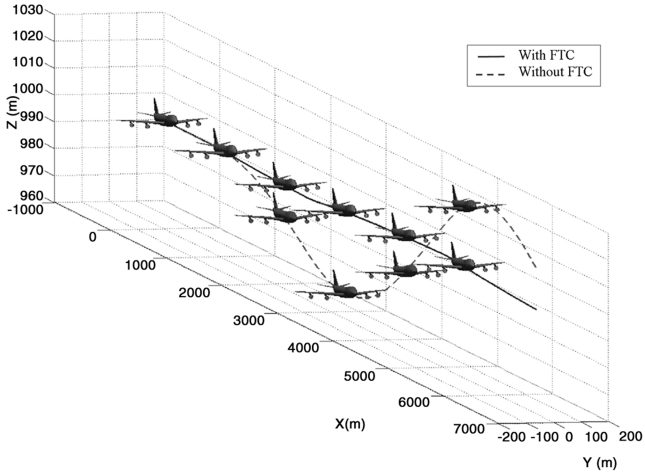

Fig. 18 Aircraft response: oscillatory THS fault.

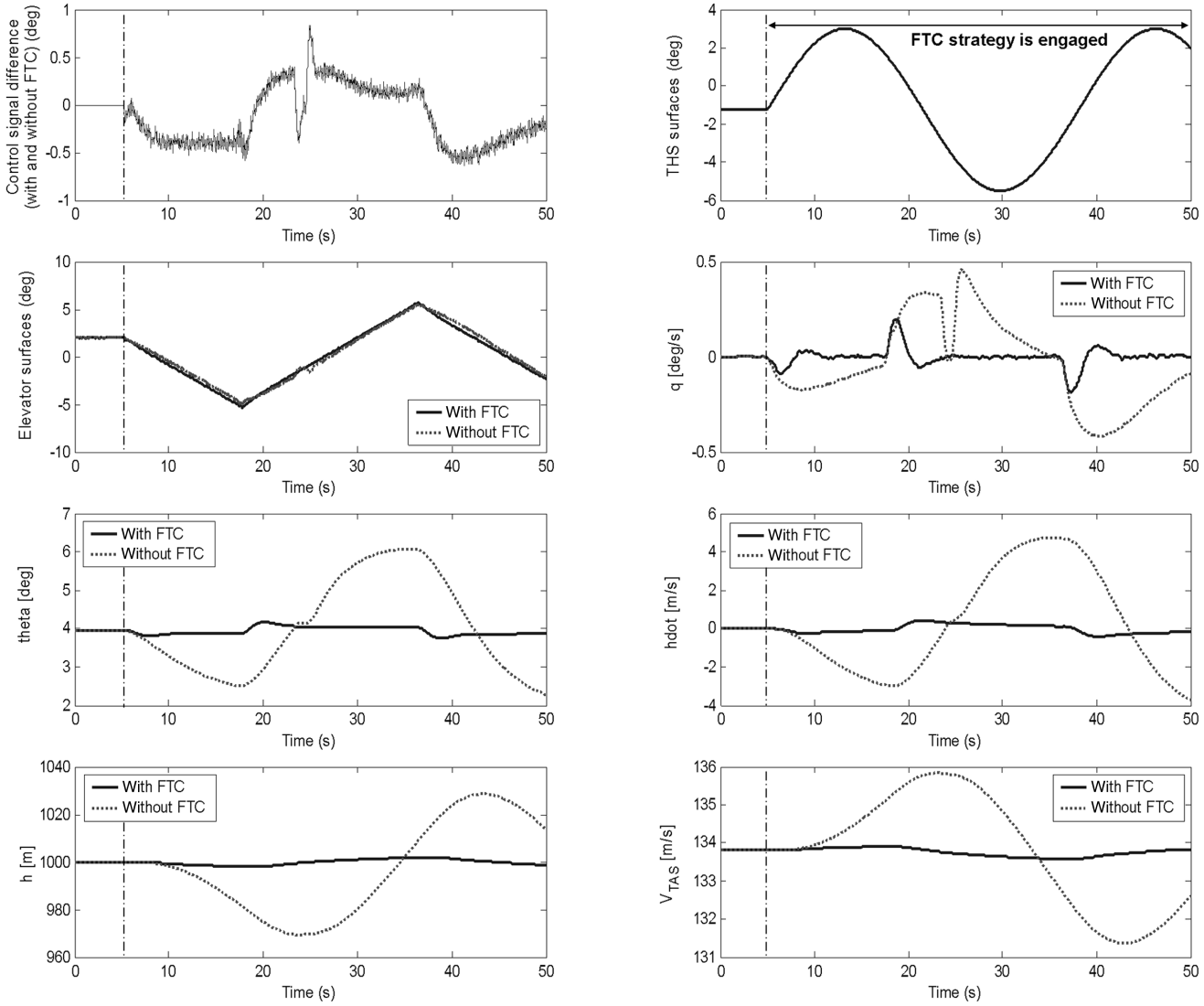

Fig. 19 Aircraft responses due to the oscillatory fault of the THS.

Figure 18 illustrates the behavior of the aircraft. It can be seen that when the FTC strategy operates, the aircraft has a flight trajectory close to the normal trajectory (i.e., the aircraft stays at the selected altitude). Figure 19 more precisely illustrates the behavior of the aircraft through the altitude h, the pitch rate q, the velocity V_{TAS}, the pitch angle θ, the altitude rate $\dot{h}$, and the control signals $\delta_{e\bullet\bullet}$. The load factor response n_z is given in Fig. 20. As can be seen, the magnitude of undesirable transients on n_z, caused by the occurrence of fault, is reduced when the FTC strategy performs. Also, the results show that the fault is compensated without violating the elevator deflection limitations.

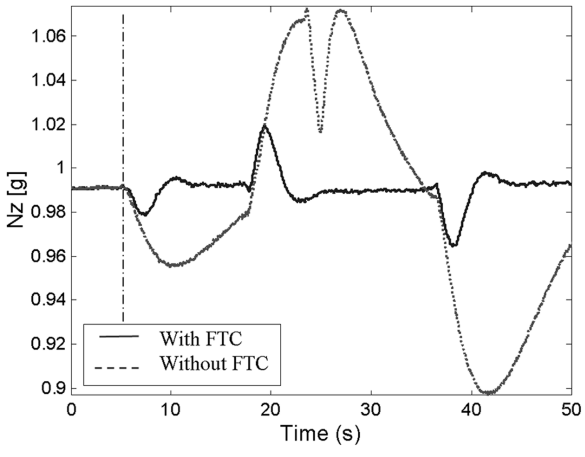

Fig. 20 Load factor: oscillatory fault of the THS.

V. Conclusions

This paper presents ongoing research undertaken within the FM-AG(16) of the GARTEUR project. This research aims at demonstrating the capability and viability of modern FDI/FTC methods on a realistic nonlinear aircraft model and to enhance critical flight safety issues. The faulty situation studied here corresponds to movement to an extreme position of the trimmable horizontal stabilizer (THS) occurring when the airplane is in normal flight. Because the design of the FDI part is not of primary interest in this work, we used information coming from available onboard detection mechanisms to activate the fault-tolerant controller. From a practical point of view, the proposed approach has some advantages over existing FTC. The proposed FTC design method uses some well-known and robust numerical tools commonly used in the robust control community (linear matrix inequalities). Another advantage is that the design of the FTC loop is done independently of the existing flight control system. In fact, the FTC system works in a way that when a fault is detected, the control law is reconfigured in real time by adding a loop activated to compensate the faults. This is an interesting aspect of this design scheme, because the overall scheme

ensures specified nominal flight performance in fault-free situations. When hardware-redundancy FDI mechanisms are not available, further investigations are necessary to extract the optimal analytical FDI unit from the set of all admissible (joint) FDI/FTC units $\bar{K}(s)$. This is a topic of future research.

Appendix A: State and Input Definition

Table A1 State definition of the Boeing 747

Symbol	Name	Unit
p	x_{NL} (1): body roll rate	rad/s
q	x_{NL} (2): body pitch rate	rad/s
r	x_{NL} (3): body yaw rate	rad/s
V_{TAS}	x_{NL} (4): true air speed	m/s
α	x_{NL} (5): angle of attack	rad
β	x_{NL} (6): angle of sideslip	rad
φ	x_{NL} (7): angle of roll	rad
θ	x_{NL} (8): angle of pitch	rad
ψ	x_{NL} (9): angle of yaw	rad
h	x_{NL} (10): altitude	m
x_e	x_{NL} (11): distance in X_e direction	m
y_e	x_{NL} (12): distance in Y_e direction	m

Table A2 Input definition of the Boeing 747

Symbol	Name	Unit
$\delta_{a\bullet\bullet}$	$\mathcal{U}_{\mathrm{NL}}$ (1): four aileron deflections	deg
$\delta_{\mathrm{sp}\bullet}$	$\mathcal{U}_{\mathrm{NL}}$ (2): 12 spoilers	deg
$\delta_{e\bullet\bullet}$	$\mathcal{U}_{\mathrm{NL}}$ (3): four elevator deflections	deg
i_h	$\mathcal{U}_{\mathrm{NL}}$ (4): stabilizer deflection	deg
$\delta_{r\bullet}$	$\mathcal{U}_{\mathrm{NL}}$ (5): two rudder deflections	deg
$\delta_{f\bullet}$	$\mathcal{U}_{\mathrm{NL}}$ (6): two flap deflections	deg
EPR$\bullet$	$\mathcal{U}_{\mathrm{NL}}$ (7): four thrust engine positions	——
gear	$\mathcal{U}_{\mathrm{NL}}$ (8): gear position	——

Appendix B: Bumpless Scheme

The activation of the FTC strategy is done using a switching logic and thus may cause some undesired phenomena such as bumps or actuator saturations. In fact, the difference between the states of nominal control law and the states of switching control law leads to these bumps. Figure B1 presents the proposed solution to manage these undesired bumps. The aim is to drive $\bar{K}(s)$ before the switch by a gain F_s, such that $\tilde{u}\mapsto 0$ and

$$\alpha \mapsto \begin{pmatrix} y \\ u_o \end{pmatrix}$$

according to

$$\begin{cases} \tilde{u} = \bar{K}\alpha \\ \alpha = F_s \begin{bmatrix} \bar{x} \\ \begin{pmatrix} y \\ u_o \end{pmatrix} \end{bmatrix} \end{cases} \tag{B1}$$

where α also denotes the control signal of $\bar{K}(s)$ before the switch, $\bar{x}$ the state vector of $\bar{K}(s)$, and F_s is the static gain to design.

Different approaches can be used to design F_s. Here, we proposed to use the idea initially proposed by [25] and applied to the FTC problem in [7]. To compute F_s, the following quadratic criterion is minimized:

$$J(\tilde{u},\alpha) = \frac{1}{2}\int_0^\infty \left\{ \tilde{u}^T W_u \tilde{u} + \left[\alpha - \begin{pmatrix} y \\ u_o \end{pmatrix}\right]^T W_e \left[\alpha - \begin{pmatrix} y \\ u_o \end{pmatrix}\right] \right\} \mathrm{d}t \tag{B2}$$

where W_u and W_e are constant positive-definite weighting matrices of appropriate dimensions. W_u and W_e allow us to define the desired objectives; that is, if it is desirable to minimize the magnitude of $\tilde{u}$, then we should choose a high value for W_u. So at switching time t_s (the time at which the fault is detected), we have $\tilde{u}(t_s)\mapsto 0$, then $u(t_s)\mapsto u_o(t_s)$. Hence, there are no bump effects. Similarly, if we want to reduce the energy of

$$\left[\alpha - \begin{pmatrix} y \\ u_o \end{pmatrix}\right]$$

then the value of W_e must be set to be high. Then at t_s, we have

$$\alpha(t_s)\mapsto \begin{pmatrix} y(t_s) \\ u_o(t_s) \end{pmatrix}$$

So there is no discontinuity between α and

$$\begin{pmatrix} y \\ u_o \end{pmatrix}$$

at switching time. This means that from a practical point of view, a tradeoff between minimizing the magnitude of $\tilde{u}$ and

$$\left[\alpha - \begin{pmatrix} y \\ u_o \end{pmatrix}\right]$$

must be done.

Once W_u and W_e have been chosen, the solution is given by (the interested reader can refer to [25] for more details)

$$F_s = \bar{N}\begin{bmatrix} (\bar{B}^T\Pi + \bar{D}^T W_u \bar{C})^T \\ [-W_e + \bar{B}^T\bar{M}(\bar{C}^T W_u \bar{D}\,\bar{N}\,W_e + \Pi\bar{B}\,\bar{N}\,W_e)]^T \end{bmatrix}^T \tag{B3}$$

where $\bar{M}$ and $\bar{N}$ are defined according to

$$\bar{M} = (\mathbf{A}^T + \Pi\mathbf{B})^{-1} \tag{B4}$$

$$\bar{N} = -(\bar{D}^T W_u \bar{D} + W_e)^{-1} \tag{B5}$$

The matrix Π is the definite-positive stationary solution of the following algebraic Riccati equation:

$$\Pi\mathbf{A} + \mathbf{A}^T\Pi + \Pi\mathbf{B}\Pi + \mathbf{C} = 0 \tag{B6}$$

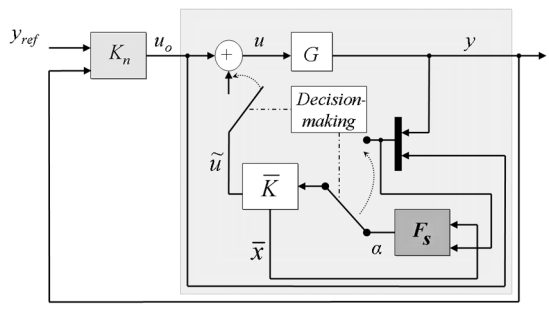

Fig. B1 FTC architecture with the bumpless scheme.

The matrices **A**, **B**, and **C** are given by

$$\mathbf{A} = \bar{A} + \bar{B}\bar{N}\bar{D}^T W_u \bar{C} \tag{B7}$$

$$\mathbf{B} = \bar{B}\bar{N}\bar{B}^T \tag{B8}$$

$$\mathbf{C} = \bar{C}^T W_u (I + \bar{D}\bar{N}\bar{D}^T W_u)\bar{C} \tag{B9}$$

where $(\bar{A}, \bar{B}, \bar{C}, \bar{D})$ denotes the state-space matrices of $\bar{K}(s)$.

Remark B.1: Using this strategy, we assume that F_s has access to the controller states $\bar{x}$. It is a modest assumption because most modern controllers will be realized in software form, and so the states will be computer variables.

Remark B.2: The proposed scheme is a unidirectional solution that permits reducing the undesirable bumpless effects for the switch from the nominal situation to the failure situation. Indeed, let t_{s_2} be the time at which the switching from the failure situation to the nominal situation is done. Just before the switch at time $t_{s_2}^-$, the controller $\bar{K}(s)$ achieves the following equation:

$$\begin{cases} \tilde{u} = \bar{K}\begin{pmatrix} y \\ u_o \end{pmatrix} \\ \alpha = F_s\left[\begin{matrix} \bar{x} \\ \begin{pmatrix} y \\ u_o \end{pmatrix} \end{matrix}\right] \end{cases} \tag{B10}$$

Then the control signal applied to the system at $t_{s_2}^-$ is given by

$$u\left(t_{s_2}^-\right) = u_0\left(t_{s_2}^-\right) + \tilde{u}\left(t_{s_2}^-\right)$$

After the switch, at time $t_{s_2}^+$, the controller $\bar{K}(s)$ is derived by Eq. (B1). Then we have

$$u(t_{s_2}^+) = u_o(t_{s_2}^+)$$

Hence, to avoid the undesirable bumps, the sufficient and necessary condition is that $\tilde{u}(t_{s_2}^-) \mapsto 0$. Unfortunately, because at time $t_{s_2}^-$ the FTC strategy is activated, it is not possible to modify on the controller $\bar{K}(s)$. The discontinuity due to the switch of the failure situation to the nominal situation is thus related to the dynamics of the FTC loop that would be activated at the switching time.

Acknowledgment

The authors would like to thank E. Prempain from the Control and Instrumentation Research Group, University of Leicester, for his helpful comments and for reviewing the initial manuscript.

References

[1] Zhang, Y., and Jiang, J., "Bibliographical Review on Reconfigurable Fault-Tolerant Control Systems," *5th IFAC Symposium on Fault Detection, Supervision and Safety of Technical Processes (SAFEPROCESS'03)*, International Federation of Automatic Control, Washington, DC, 2003, pp. 265–276.

[2] Zhang, Y. M., and Jiang, J., "Issues on Integration of Fault Diagnosis and Reconfigurable Control in Active Fault-Tolerant Control Systems," *6th IFAC Symposium on Fault Detection, Supervision and Safety of Technical Processes (SAFEPROCESS '06)* [CD-ROM], International Federation of Automatic Control, Washington, DC, 2006.

[3] Steinberg, M., "Historical Overview of Research in Reconfigurable Flight Control," *Proceedings of the Institution of Mechanical Engineers, Part G (Journal of Aerospace Engineering)*, Vol. 219, No. 4, 2005, pp. 263–275. doi:10.1243/095441005X30379

[4] Staroswiecki, M., and Gehin, A. L., "From Control to Supervision," *Annual Reviews in Control*, Vol. 25, 2001, pp. 1–11. doi:10.1016/S1367-5788(01)00002-5

[5] Moerder, D. D., Halyo, N., Broussard, J. R., and Caglayan, A. K., "Application of Precomputed Control Laws In a Reconfigurable Aircraft Flight Control System," *Journal of Guidance, Control, and Dynamics*, Vol. 12, No. 3, 1989, pp. 325–333.

[6] Huzmezan, M., and Maciejowski, J. M., "Reconfigurable Flight Control of a High Incidence Research Model Using Predictive Control," *International Conference on Control*, Inst. of Electrical and Electronics Engineers, Piscataway, NJ, 1998, pp. 1169–1174.

[7] Chen, J., and Patton, R. J., "Fault-Tolerant Control Using LMI Design," *European Control Conference (ECC'01)*, Inst. of Electrical and Electronics Engineers, Piscataway, NJ, 2001.

[8] Cieslak, J., Henry, D., and Zolghadri, A., "A Methodology for the Design of Active Fault Tolerant Control Systems," *6th IFAC Symposium on Fault Detection, Supervision and Safety of Technical Processes (SAFEPROCESS '06)* [CD-ROM], International Federation of Automatic Control, Washington, DC, 2006.

[9] Maki, M., Jiang, J., and Hagino, K., "A Stability Guaranteed Active Fault-Tolerant Control System Against Actuator Failures," *Proceedings of the 40th IEEE Conference on Decision and Control*, Inst. of Electrical and Electronics Engineers, Piscataway, NJ, Dec. 2001, pp. 1893–1898.

[10] Staroswiecki, M., Yang, H., and Jiang, B., "Progressive Accommodation of Aircraft Actuator Faults," *6th IFAC Symposium on Fault Detection, Supervision and Safety of Technical Processes (SAFEPROCESS '06)* [CD-ROM], International Federation of Automatic Control, Washington, DC, 2006.

[11] Campos-Delagado, D. U., Palacios, E. R., and Espinoza-Trejo, D. R., "Fault Accommodation Strategy for LTI Systems Based on GIMC Structure: Additive Faults," *44th IEEE Conference on Decision and Control*, Inst. of Electrical and Electronics Engineers, Piscataway, NJ, 2005, pp. 6292–6297.

[12] Neimann, H., and Stoustrup, J., "Passive Fault Tolerant Control of a Double Inverted Pendulum: A Case Study," *Control Engineering Practice*, Vol. 13, No. 8, 2005, pp. 1047–1059. doi:10.1016/j.conengprac.2004.11.002

[13] Ganguli, S., Marcos, A., and Balas, G., "Reconfigurable LPV Control Design for B-747-100/200 Longitudinal Axis," *Proceedings of the American Control Conference*, Vol. 5, Inst. of Electrical and Electronics Engineers, Piscataway, NJ, 2002, pp. 3612–361710.1109/ACC.2002.1024489.

[14] Gaspar, P., Szaszi, I., and Bokor, J., "Reconfigurable Control Structure to Prevent the Rollover Of Heavy Vehicles," *Control Engineering Practice*, Vol. 13, No. 6, 2005, pp. 699–711. doi:10.1016/j.conengprac.2004.06.003

[15] Van der linden, C. A. A. M., "DASMAT-Delft University Aircraft Simulation Model and Analysis Tool," Delft Univ. of Technology, Rept LR-781, Delft, The Netherlands, 1996.

[16] Smaili, M. H., "FLIGHTLAB 747 Benchmark for Advanced Flight Control Engineering v4.03," Delft Univ. of Technology, Delft, The Netherlands, 1999.

[17] Lombaerts, T. J. J., Joosten, D. A., Breeman, J., Smaili, H., Van den Boom, T. J. J., Chuk, Q. P., Mulder, J. A., and Verhaegen, M., "Assessment Criteria as Specifications for Reconfiguring Control," AIAA Guidance, Navigation, and Control Conference and Exhibit, Keystone, CO, AIAA Paper 2006-6331, 21–24 Aug. 2006.

[18] Smaili, M. H., Breeman, J., Lombaerts, T. J. J., and Joosten, D. A., "A Simulation Benchmark for Integrated Fault Tolerant Flight Control Evaluation," AIAA Modeling and Simulation Technologies Conference, AIAA Paper 2006-6471, Aug. 2006.

[19] Zhou, K., and Ren, Z., "A New Controller Architecture for High Performance, Robust, and Fault-Tolerant Control," *IEEE Transactions on Automatic Control*, Vol. 46, No. 10, 2001, pp. 1613–1618. doi:10.1109/9.956059

[20] Marcos, A., "A Linear Parameter Varying Model of the Boeing 747-100/200 Longitudinal Motion," M.S. Thesis, Univ. of Minnesota, Minneapolis, MN, 2001.

[21] Hanke, C., and Nordwall, D. R., "The Simulation of a Jumbo Jet Transport Aircraft," Vol. 2, The Boeing Company, Rept. D6-30643, 1970.

[22] Chilali, M., and Gahinet, P., "H_∞ Design with Pole Placement Constraints: An LMI Approach," *IEEE Transactions on Automatic Control*, Vol. 41, No. 3, Mar. 1996, pp. 358–367. doi:10.1109/9.486637

[23] Scherer, C., Gahinet, P., and Chilali, M., "Multiobjective Output-Feedback Control via LMI Optimization," *IEEE Transactions on Automatic Control*, Vol. 42, No. 7, July 1997, pp. 896–911. doi:10.1109/9.599969

[24] Toh, K. C., Todd, M. J., and Tütüncü, R. H., "SDPT3 a MATLAB

Software Package for Semidefinite Programming," *Optimization Methods and Software*, Gordon & Breach, Berkshire, England, U.K., 1998.

[25] Turner, M. C., and Walker, D. J., "Linear Quadratic Bumpless Transfer," *Automatica*, Vol. 36, No. 8, 2000, pp. 1089–1101. doi:10.1016/S0005-1098(00)00021-2